

# QCD corrections to hadronic WWZ production with leptonic decays

V. Hankele and D. Zeppenfeld

*Institut für Theoretische Physik, Universität Karlsruhe, P.O.Box 6980, 76128 Karlsruhe, Germany*

## Abstract

Multi-lepton signatures appear in many new physics searches at the Large Hadron Collider. We here consider WWZ production with subsequent leptonic decay of the three vector bosons as a SM source of multi-lepton events. We have calculated the next-to-leading order QCD corrections for the full  $pp \rightarrow 6$  lepton production cross sections in hadronic collisions. Results have been implemented in the form of a flexible parton-level Monte-Carlo program which allows to calculate the QCD corrections for arbitrary distributions and acceptance cuts.

# 1 Introduction

With the start of the CERN Large Hadron Collider (LHC) a trove of new data is anticipated, which can be used to search for new physics and also to further probe the Standard Model (SM). For the interpretation of these data, precise predictions for both the desired signal processes and backgrounds are needed, and this necessitates the calculation of next-to-leading order (NLO) QCD corrections. In order to determine cross sections for non-trivial acceptance cuts, it is most useful to cast these NLO calculations into fully flexible Monte-Carlo programs which can calculate cross sections as well as distributions.

WWZ production with subsequent leptonic decay of the vector bosons is a background to supersymmetric processes with several leptons in the final state. In addition, it is an excellent probe of the quartic electroweak  $W^+W^-\gamma\gamma$ ,  $W^+W^-Z\gamma$  and  $W^+W^-ZZ$  couplings. Constraints for some of these couplings are already available from the Large Electron Positron collider (LEP) at CERN [1] and analogous measurements have been suggested for proton antiproton collisions at the Fermilab Tevatron collider [2]. However, the LHC will be able to improve these measurements considerably and therefore more accurate predictions are needed [3]. As we will see, QCD corrections increase the WWZ cross section by more than 70% and, thus, any quantitative measurement of quartic couplings will have to take QCD corrections into account. This sizable enhancement is not surprising in view of the similarity with diboson production [4, 5]. Furthermore QCD corrections to ZZZ production at the LHC have already been calculated and increase the LO cross section by about 50% [6].

We here present first results on the NLO QCD corrections to the full  $2 \rightarrow 6$  process  $pp \rightarrow \nu_e e^+ \mu^- \bar{\nu}_\mu \tau^- \tau^+$  (or any other combination of leptons from three distinct families). All resonant and non-resonant matrix elements as well as the spin correlations of the final state leptons are included in our calculation. For simplicity, we neglect any identical lepton effects which might appear when using the results for final states with leptons from one or two generations only. The calculation is performed with the Catani-Seymour subtraction algorithm [7] and uses the virtual amplitudes derived in Refs. [8, 9]. Further details of the calculation and the checks we performed will be given in section 2. First determinations of cross sections, distributions and  $K$ -factors are presented in section 3.

## 2 The Calculation

We have considered in our calculation the full set of Feynman graphs for the process  $pp \rightarrow \nu_{\ell_1} \ell_1^+ \ell_2^- \bar{\nu}_{\ell_2} \ell_3^- \ell_3^+$  up to order  $\alpha_s \alpha^6$ . This includes the Higgs contribution and all off-shell diagrams. However, interference terms due to identical particles in the final state have been neglected. Including such effects at LO we find that this is an excellent approximation: LO cross sections change by less than 0.1% when interference terms are integrated over the Breit Wigner peaks. Interference terms show strong cancellations between contributions below and above the Breit Wigner peaks, but even their absolute values contribute at the few percent level only, which is below the scale variation of our final NLO cross sections.

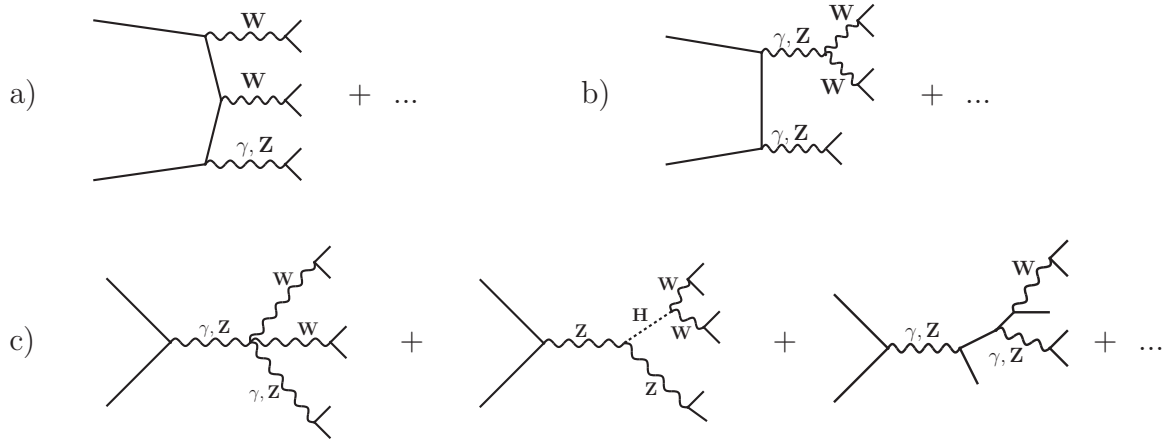


Figure 1: *Some representative tree-level Feynman diagrams of the process  $pp \rightarrow 4\ell + 2\nu$ . They show the three different topologies appearing in this calculation.*

We also neglect any fermion mass effects. In particular, the Higgs Yukawa coupling to tau leptons is set to zero. Because of the large number of Feynman diagrams we use the helicity method of Ref. [10] for the evaluation of the matrix elements.

Some representative tree-level Feynman diagrams are given in Fig. 1. The 181 tree-level graphs can be grouped into three distinct topologies. In Fig. 1a three vector bosons with subsequent decay are emitted from the quark line. The polarization vectors of these vector bosons are the decay currents describing the respective decay leptons, and these decay currents appear in many different Feynman graphs. In order to speed up the calculation, they are determined numerically at the beginning of the evaluation of the matrix elements for a given phase space point and reused wherever they appear. In Fig. 1b two vector bosons are attached to a quark line and then decay into two or four leptons. All the Feynman graphs for a 4-lepton decay can again be combined to an effective polarization vector. For all subprocesses like  $u\bar{u} \rightarrow 4\ell + 2\nu$  or  $\bar{d}d \rightarrow 4\ell + 2\nu$  these polarization vectors are the same for one specific phase space point and they do not depend on the quark polarization. Furthermore they appear in various Feynman diagrams. In our code these polarization vectors are therefore calculated once per phase space point, stored and reused wherever possible. The last topology is the one where only one vector boson is attached to the quark line. The polarization vector corresponding to the “decay” of this virtual vector boson can be calculated once per phase space point, stored and reused. The method of precalculating effective polarization vectors renders our code for the Born processes about 4 times faster than a direct evaluation with `MadGraph` [11].

The full NLO cross section consists of real emission contributions, virtual contributions and a finite remainder from the factorization of collinear singularities into the parton distribution functions (pdfs). The real emission contributions have to be integrated over an  $(m+1)$ -particle phase space with  $m = 6$  leptons, and the other two contributions only involve

an  $m$ -particle phase space.

$$\sigma^{NLO} = \int_{m+1} d\sigma^R + \int_m d\sigma^V + \int_m d\sigma^C \quad (2.1)$$

The virtual and the real emission contribution are separately infrared divergent and only their sum gives a well defined finite result. We have used the dipole subtraction algorithm proposed by Catani and Seymour [7] in order to handle these divergencies in our Monte-Carlo program.

The real emission matrix elements can be obtained from the Born level matrix elements by either attaching a gluon to a quark line or having a gluon in the initial state which then splits into a quark anti-quark pair. The method of precalculating the effective polarization vectors for leptonic decays, described above for the tree-level diagrams, has also been used for the more complicated real emission diagrams. Here an increase in computational speed by about a factor of 12 is reached.

The “virtual” contribution consists of the square of tree-level diagrams and the interference between tree-level diagrams and the virtual one-loop diagrams. In the calculation of the one-loop diagrams, three different types of contributions corresponding to the three topologies in Fig. 1 appear. For the simplest topology, with one vector boson attached to the quark line, only vertex corrections appear. In this case the one-loop contribution is proportional to the Born matrix element. The second topology, Fig. 1b, leads to propagator corrections, vertex corrections and boxes. In the calculation, the sum of these corrections to one specific tree-level subamplitude is grouped together and will be called a boxline contribution in the following. The most challenging topology, Fig. 1a, leads to quark propagator corrections, vertex corrections, boxes and pentagons. As in the previous case the sum of all these corrections to one specific tree level Feynman graph is grouped together and called pentline contribution in the following.

The boxline contribution has the same structure as in the vector boson fusion process  $qq \rightarrow Vqq$ , which was considered in Ref. [8]. Similarly the pentline contribution is obtained by crossing from the results of Ref. [9], where QCD corrections to the vector boson fusion processes  $qq \rightarrow qqVV$  were determined. The singular contributions of all of these three types of virtual contributions are proportional to the Born matrix element and the complete virtual one-loop contribution for the three topologies is given by

$$M_V = \tilde{M}_V + \frac{\alpha_S}{4\pi} C_F \left( \frac{4\pi\mu^2}{s} \right)^\epsilon \Gamma(1 + \epsilon) \left[ -\frac{2}{\epsilon^2} - \frac{3}{\epsilon} - 8 + \frac{4}{3} \pi^2 \right] M_B, \quad (2.2)$$

where  $M_B$  denotes the full Born amplitude,  $s$  is the square of the partonic center of mass energy, i.e. it corresponds to the invariant mass of the 6-lepton system, and  $\tilde{M}_V$  is the finite part of the virtual boxline and pentline amplitudes, which are obtained by crossing and analytic continuation from the results of Refs. [8, 9]. In the calculation of the boxline routine the usual Passarino-Veltman tensor decomposition [12] is applied, whereas in the pentline routine the method proposed by Denner and Dittmaier [13] has been used for the tensor coefficients of pentagon diagrams.

Since the pentagon routines are quite time consuming we have employed a method suggested in Ref. [9] to reduce the magnitude of the true pentagon contribution. It is possible to shift the polarization vectors or respectively the decay currents of the vector bosons by terms proportional to their momenta,

$$\epsilon_V^\mu = x_V q_V^\mu + \tilde{\epsilon}_V^\mu. \quad (2.3)$$

The pentagons contracted with the momenta instead of the polarization vector (terms proportional to  $x_V$ ) can then be expressed in terms of boxes via Ward identities for the loop integrals and the magnitude of the remaining pentagon contribution is reduced to a numerically less challenging level. In practice we choose

$$\tilde{\epsilon}_{W^\pm} \cdot (q_{W^+} + q_{W^-}) = 0 \quad (2.4)$$

which means that the shifted polarization vectors have zero time component in the center of mass system of the  $W$ -pair.

We have checked our calculation at numerous levels. All the matrix elements for the LO process and the real emission part have been compared with **MadGraph** [11] output. For individual matrix elements we find agreement at the  $10^{-15}$  level. In addition, the total LO cross section has been checked against **MadEvent** [11] and **HELAC** [14]. For the real emission part the LO process  $pp \rightarrow 4\ell + 2\nu + j$  has been compared against **MadEvent**. Results agree within the statistical accuracy of the Monte-Carlo runs (0.5% for **MadEvent** and 0.2% for **HELAC**).

The finite collinear terms have been checked by exploiting the fact that they are generic for all Drell-Yan type processes and hence should be exactly the same for  $WW$  production. We have independently programmed NLO QCD corrections for  $WW$  production and compared our results with **MCFM** [5]. We find full agreement for different factorization and renormalization scales. As a further check we have taken advantage of the fact that we can integrate terms proportional to the Born matrix element either together with the real emission part, by integration over the  $(m+1)$ -particle phase space, or together with the virtual part, by integrating over the  $m$ -particle phase space. Resulting cross sections are independent of this choice of procedure.

For the virtual contributions Ward identity tests have been implemented as a flag for numerically unstable evaluation of tensor coefficients. In the case of pentagon diagrams, for example, the pentline contribution can be expressed in terms of boxes if one of the external polarization vectors is replaced by its momentum. We discard the pentline contribution at phase space points where the two ways of calculating these terms disagree by more than 10%. The resultant loss in cross section is negligible: extrapolating its size we estimate the resultant relative error on the NLO cross section to be below  $10^{-4}$ .

Many of the critical elements of our calculation also appear in the related process  $pp \rightarrow ZZZ$  for which NLO QCD corrections have recently been presented in Ref. [6], albeit without further decay of the leptons and neglecting any Higgs contributions. As a last and very powerful test we have modified our code to describe  $ZZZ$  instead of  $WWZ$  production and checked against the results of Ref. [6]. Using the same pdfs and  $\alpha_s(m_Z) = 0.119$  at NLO we find complete agreement for all of the given renormalization and factorization scales.

### 3 Results

The complete next-to-leading order calculation has been implemented in the framework of a fully flexible Monte-Carlo program, **VBFNLO**, which then has been used to determine the QCD corrections to WWZ production at the LHC. For the generation of our results we set the electroweak parameters to the following values:

$$\begin{aligned} m_W &= 80.419 \text{ GeV} & m_Z &= 91.188 \text{ GeV} \\ G_F &= 1.16639 \cdot 10^{-5} \text{ GeV}^{-2} & m_H &= 120 \text{ GeV}. \end{aligned} \quad (3.1)$$

The other electroweak parameters,  $\alpha^{-1} = 132.507$  and  $\sin^2(\theta_W) = 0.22225$ , are calculated in the program by using LO electroweak relations. The default value for the renormalization and factorization scale is the invariant WWZ mass, which is given by

$$\mu_F = \mu_R = \sqrt{(p_{\ell_1} + p_{\ell_2} + p_{\ell_3} + p_{\ell_4} + p_{\nu_1} + p_{\nu_2})^2}. \quad (3.2)$$

For scale variation studies of the total cross section, we also consider fixed renormalization and factorization scales, which we set as  $\mu_F = \mu_R = \xi \cdot m_Z$ . We use the CTEQ6M parton distribution with  $\alpha_s(m_Z) = 0.118$  at NLO and CTEQ6L1 for the LO calculation [15]. All fermions are treated as massless and we do not consider contributions involving bottom and top quarks. The CKM matrix is approximated by a unit matrix throughout, which is appropriate when neglecting fermion mass effects in a neutral Drell-Yan type process.

In order to keep most of the cross section we apply only minimal cuts to the final state leptons. This means that besides a cut on the minimal transverse momentum and the maximal rapidity of the charged leptons we only require that the invariant dilepton mass,  $m_{\ell\ell}$ , of any combination of the charged leptons is larger than 15 GeV, thus steering clear of the virtual photon singularity in  $\gamma^* \rightarrow \ell^+ \ell^-$  at low  $m_{\ell\ell}$ . Specifically, we require

$$p_{T_\ell} > 10 \text{ GeV} \quad |y_\ell| < 2.5 \quad m_{\ell\ell} > 15 \text{ GeV} \quad (3.3)$$

in all subsequent figures. All results given here have been calculated for the process  $pp \rightarrow \nu_e e^+ \mu^- \bar{\nu}_\mu \tau^- \tau^+$ , i.e. interference terms due to identical particles have been neglected. In order to obtain cross sections for the phenomenologically more interesting case of final states with four electrons and/or muons, we have multiplied these results by a combinatorial factor of 8 in all figures.

In the left panel of Fig. 2 the scale dependence of the cross section at LO and NLO is shown. The LO scale dependence severely underestimates the uncertainties of the LO cross section due to the fact that no  $\alpha_S$  appears in the LO calculation and that the pdfs are determined in a Feynman- $x$  range of small factorization scale dependence. The right panel of Fig. 2 shows the scale dependence of the different contributions to the NLO cross section. The virtual contribution is split up into one part proportional to the Born matrix element, one part with boxline contributions and a third part which includes only the true pentline contribution after the reduction described in equations (2.3), (2.4). This pentagon contribution amounts to 1 - 2% of the total NLO cross section. The real emission contribution

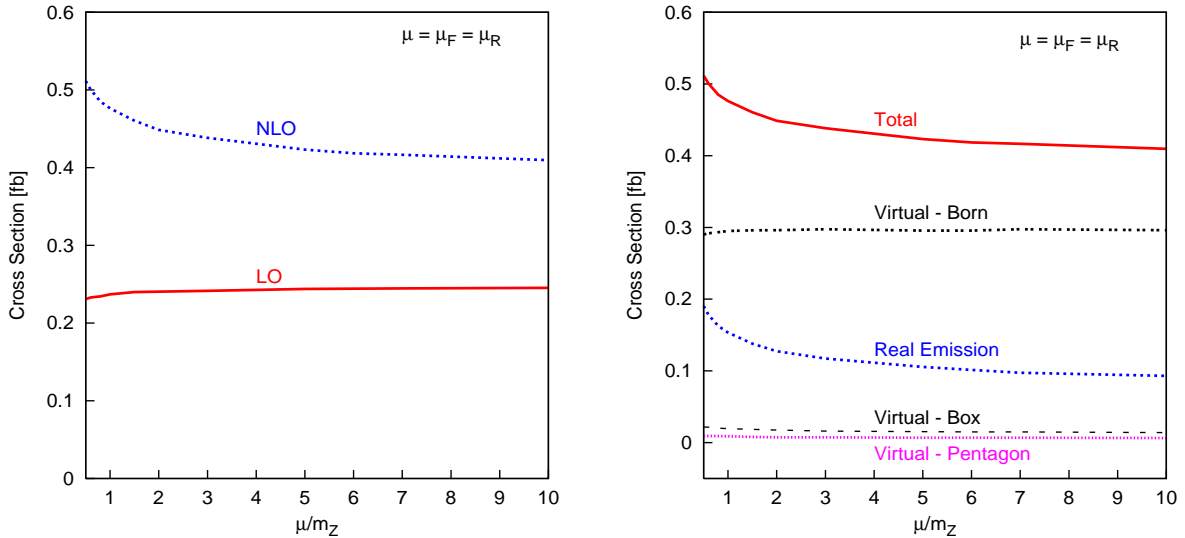


Figure 2: *Left:* Scale dependence of the total cross section for  $pp \rightarrow WWZ \rightarrow 4\ell + \cancel{p}_T$  at LO and NLO for  $m_H = 120$  GeV and the cuts of Eq. (3.3). The factorization and renormalization scales are taken at a fixed value which is varied in the range from  $0.5 \cdot m_Z$  to  $10 \cdot m_Z$ . *Right:* Same as in the left panel but for the different NLO contributions.

in the plot includes the additional finite terms from the factorization of collinear singularities into the pdfs. The scale dependence of the NLO cross section is mainly due this real emission contribution.

The  $K$ -factor, defined as the ratio of the NLO cross section over the LO cross section strongly depends on the factorization and renormalization scale. It is shown in Fig. 2 for a fixed scale choice,  $\mu_R = \mu_F = \xi \cdot m_Z$ . One finds variations of the  $K$ -factor between 1.7 (for large scales) and 2.2 (for small scales). A qualitatively similar scale dependence is found if instead of the  $Z$ -mass the invariant 6-lepton mass as given in Eq. (3.2) is taken as reference scale choice. The mean value of this dynamical reference scale is substantially larger than the  $Z$ -mass and the  $K$ -factor for  $\mu_F = \mu_R = m_{WWZ}$  is 1.74. Since the  $WWZ$  invariant mass is the scale of the Drell-Yan type subdiagrams in Fig. 1, it may be considered the most natural scale choice in the present calculation. We leave a more thorough investigation of scale dependence of the NLO cross section to a future publication [16], however.

The size of the NLO QCD corrections shows a marked phase space dependence. Two examples are shown in the remaining figures. In the left panel of Fig. 3 the transverse momentum distribution of the highest- $p_T$  charged lepton is shown for the cuts given in Eq. (3.3). The right panel shows the differential  $K$ -factor, defined as

$$K = \frac{d\sigma^{NLO}/dx}{d\sigma^{LO}/dx}. \quad (3.4)$$

The  $K$ -factor increases with  $p_T$  by almost a factor 2, indicating that a simple multiplication with a constant overall  $K$ -factor would seriously change the shape of lepton  $p_T$  distributions. A somewhat more benign behavior is found for the 4-lepton invariant mass distribution which

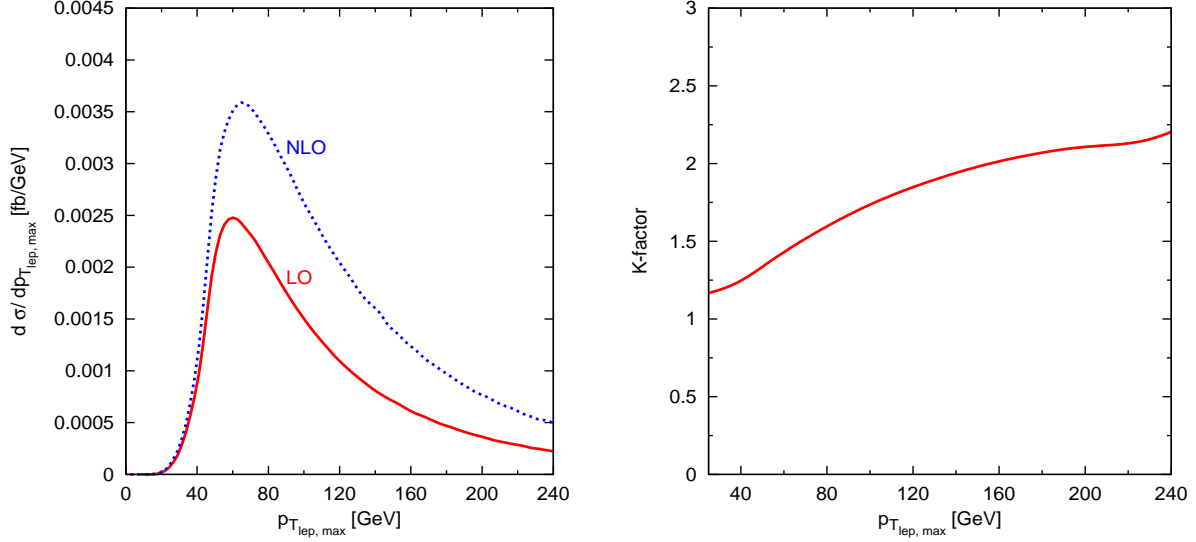


Figure 3: *Left:* Transverse momentum distribution of the highest- $p_T$  charged lepton for  $m_H = 120$  GeV,  $\mu_F = \mu_R = m_{WWZ}$  as given in Eq. (3.2) and the cuts given in Eq. (3.3) at LO and NLO. *Right:* Differential  $K$ -factor as defined in Eq. (3.4) for the two distributions in the left panel.

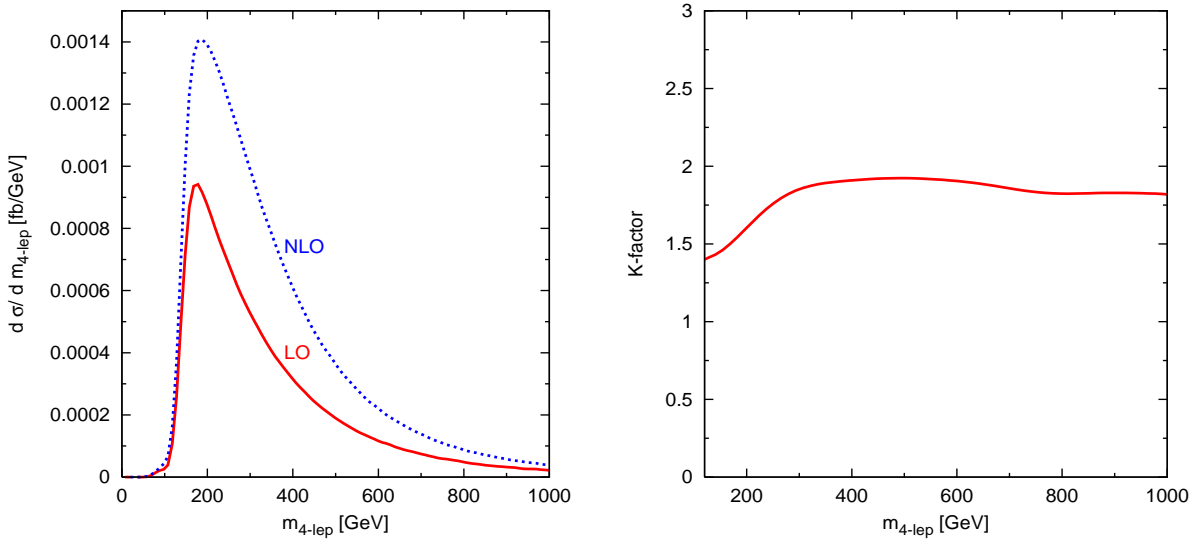


Figure 4: *Left:* Invariant mass distribution of the four charged leptons for  $m_H = 120$  GeV,  $\mu_F = \mu_R = m_{WWZ}$  and the cuts given in Eq. (3.3) at LO and NLO. *Right:* Differential  $K$ -factor as defined in Eq. (3.4) for the two distributions in the left panel.



is shown in Fig. 4. Here the differential  $K$ -factor varies between 1.4 and 1.9 and most of the rise is in the threshold region. For 4-lepton invariant masses above 250 GeV a constant  $K$ -factor would be an adequate approximation for the  $m_{4\ell}$  distribution.

## 4 Conclusions

WWZ production with subsequent leptonic decays is an important source of multi-lepton events and of great interest for the measurement of quartic electroweak couplings at the LHC. In this letter we have presented first results on the NLO QCD corrections to the process  $pp \rightarrow \nu_{\ell_1} \ell_1^+ \ell_2^- \bar{\nu}_{\ell_2} \ell_3^- \ell_3^+$ . For the WWZ invariant mass as renormalization and factorization scale, the overall  $K$ -factor is about 1.7 and therefore has to be taken into account in any analysis involving WWZ production.

The scale dependence of the NLO cross section is substantially larger than the variation observed for the LO results. This can be quantified by increasing and lowering the renormalization and factorization scale by a factor of 2 around  $3 \cdot m_Z$  as central value. At LO the scale dependence is very small with a variation of less than  $\pm 1.5\%$ , whereas at NLO variations of  $\pm 5\%$  appear. The NLO uncertainties which are indicated by the scale dependence are, thus, typical for a NLO QCD prediction, while the LO case must be considered as anomalous. Indeed, the WWZ cross section provides another example where the scale variation of a LO cross section does not give a good estimate for the corrections due to higher order effects.

The NLO QCD corrections do not only change the normalization of the total WWZ cross section, they also lead to substantial shape changes of distributions: the differential  $K$ -factors show a sizable variation over phase space. Reliable modeling of the lepton distributions arising from WWZ production at the LHC thus requires the inclusion of NLO QCD corrections. These corrections are now available in the form of a flexible parton level Monte Carlo program, which will be incorporated into the publicly available VBFNLO package [17] in the near future.

## Acknowledgments

We would like to thank Frank Petriello for his help in comparing the ZZZ production cross sections, Malgorzata Worek for the comparison with HELAC and Carlo Oleari for many useful discussions. This research was supported by the Deutsche Forschungsgemeinschaft via the Sonderforschungsbereich/Transregio SFB/TR-9 “Computational Particle Physics” and the Graduiertenkolleg “High Energy Physics and Particle Astrophysics”.

## References

- [1] J. Alcaraz *et al.* [ALEPH Collaboration], arXiv:hep-ex/0612034.
- [2] See for example T. Han and R. Sobey, Phys. Rev. D **52** (1995) 6302 [arXiv:hep-ph/9507409]; P. J. Dervan, A. Signer, W. J. Stirling and A. Werthenbach, J. Phys. G **26** (2000) 607 [arXiv:hep-ph/0002175].
- [3] See for example O. J. P. Eboli, M. C. Gonzalez-Garcia, S. M. Lietti and S. F. Novaes, Phys. Rev. D **63** (2001) 075008 [arXiv:hep-ph/0009262]; D. Green, arXiv:hep-ex/0310004.
- [4] See for example J. Ohnemus, arXiv:hep-ph/9503389; L. J. Dixon, Z. Kunszt and A. Signer, Phys. Rev. D **60** (1999) 114037 [arXiv:hep-ph/9907305]; L. J. Dixon, Z. Kunszt and A. Signer, Nucl. Phys. B **531** (1998) 3 [arXiv:hep-ph/9803250]; J. Ohnemus, Phys. Rev. D **50** (1994) 1931 [arXiv:hep-ph/9403331].
- [5] J. M. Campbell and R. K. Ellis, Phys. Rev. D **60** (1999) 113006 [arXiv:hep-ph/9905386].
- [6] A. Lazopoulos, K. Melnikov and F. Petriello, Phys. Rev. D **76** (2007) 014001 [arXiv:hep-ph/0703273].
- [7] S. Catani and M. H. Seymour, Nucl. Phys. B **485** (1997) 291 [Erratum-ibid. B **510** (1998) 503] [arXiv:hep-ph/9605323].
- [8] C. Oleari and D. Zeppenfeld, Phys. Rev. D **69** (2004) 093004 [arXiv:hep-ph/0310156].
- [9] B. Jager, C. Oleari and D. Zeppenfeld, JHEP **0607** (2006) 015 [arXiv:hep-ph/0603177]; G. Bozzi, B. Jager, C. Oleari and D. Zeppenfeld, Phys. Rev. D **75** (2007) 073004 [arXiv:hep-ph/0701105].
- [10] K. Hagiwara and D. Zeppenfeld, Nucl. Phys. B **274** (1986) 1; K. Hagiwara and D. Zeppenfeld, Nucl. Phys. B **313** (1989) 560.
- [11] T. Stelzer and W. F. Long, Comput. Phys. Commun. **81** (1994) 357 [arXiv:hep-ph/9401258]; F. Maltoni and T. Stelzer, JHEP **0302** (2003) 027 [arXiv:hep-ph/0208156].
- [12] G. Passarino and M. J. G. Veltman, Nucl. Phys. B **160** (1979) 151.
- [13] A. Denner and S. Dittmaier, Nucl. Phys. B **658**, 175 (2003) [arXiv:hep-ph/0212259]; A. Denner and S. Dittmaier, Nucl. Phys. B **734**, 62 (2006) [arXiv:hep-ph/0509141].
- [14] A. Cafarella, C. G. Papadopoulos and M. Worek, arXiv:0710.2427 [hep-ph]; C. G. Papadopoulos and M. Worek, arXiv:hep-ph/0606320; A. Kanaki and C. G. Papadopoulos, Comput. Phys. Commun. **132** (2000) 306 [arXiv:hep-ph/0002082].
- [15] J. Pumplin, D. R. Stump, J. Huston, H. L. Lai, P. Nadolsky and W. K. Tung, JHEP **0207** (2002) 012 [arXiv:hep-ph/0201195].

- [16] V. Hankele and D. Zeppenfeld, in preparation.
- [17] The VBFNLO program is available at  
<http://www-itp.particle.uni-karlsruhe.de/~vbfnoweb/>